Precursor forms of cavity solitons in nonlinear semiconductor microresonators

Isabelle Ganne, Gintas Slekys, Isabelle Sagnes, and Robert Kuszelewicz*
Laboratoire de Photonique et de Nanostructures, Centre National de la Recherche Scientifique–UPR020, route de Nozay, 91460 Marcoussis, France
(Received 14 January 2002; published 30 December 2002)

We study the transverse nonlinear dynamics of bulk and multi-quantum well AlGaAs microresonators, in the mixed dispersive and saturable absorptive regime, slightly below the band-gap edge energy. With a Gaussian beam excitation we observe strongly localized states of various shapes, bright or dark in reflection. Their dynamics appears to be ruled by strong thermally induced nonlinear mechanisms, acting as a dressing mechanism for electronic nonlinearities. Precursor forms of cavity solitons are also identified.

DOI: 10.1103/PhysRevE.66.066613 PACS number(s): 42.65.Tg, 42.65.Sf, 42.65.Pc, 47.54.+r

I. INTRODUCTION

Optical bistable systems have been known for more than twenty years [1–3] to constitute the basic substrate on which lay down the realization of massively parallel all-optical binary systems [4]. As in the early systems, only the spatially homogeneous response of plane nonlinear resonators was originally considered [2], the delimitation of parallel independent channels required the use of irreversible mechanical or chemical actions. During the 1980's, despite the usual Gaussian character of the excitation beam, a large amount of investigations on bistability in Kerr-like materials was conducted within the frame of a plane wave (PW) excitation [5]. Transverse effects were considered as limitations and their study aimed at the reduction of their perturbing effects. More recent studies performed during the last decade have extended the field of investigation to the case of a spatially inhomogeneous response, taking fully into account transverse mechanisms and giving rise to the rapidly increasing field of transverse nonlinear optics. In such systems, a strong enrichment of the spatio-temporal physics is introduced by the interplay of nonlinear light propagation with transverse mechanisms that can lead to self-organized optical states emerging in the form of global patterns or autonomous localized structures called cavity solitons (CS) [6]. This process results from a balance between the counteracting effects of defocusing mechanisms provided by optical diffraction and transverse diffusion of the material excitation states, and a focusing mechanism introduced by an optical nonlinearity, in the form of the saturation of the absorption or a positive dispersive nonlinearity. In order to host stable localized states or periodic patterns, specific systems based on planar optical resonators have been proposed. A nonlinear cavity provides a feedback contribution and thereby an additional mechanism for stabilizing such features as cavity solitons [7–9]. CS have also been predicted in optical parametric oscillator associated with a saturable absorber [10]. Though, these cavity solitons have been demonstrated in two-dimensional transverse systems solely in macroscopic cavities filled with slow response materials [11]. They have been also demonstrated in slightly different systems such as a laser cavity [12], or in a sodium atomic vapors cell with a simple feedback mirror [13].

In microresonators, optical self-organization of the nonlinear response naturally points to applications in all-optical information processing domains, through the ability to form controlled arrays of optical information bits [8]. Moreover, it proposes quite innovative processing schemes including reconfigurable arrays [14] and operation modes of the cellular automaton type. In optical information processing, III-V semiconductor microresonators have been widely used to realize functional applications, such as sources, amplifiers, modulators and bistable memory elements [5]. This is for a large part due to the combination of micrometer space-scale integration, the reasonably fast characteristic times on the nanosecond time scale, large material flexibility, and intrinsic stability of their geometrical properties. Thus semiconductor-based systems can serve for high bit-rate processing. In addition, III-V semiconductors display either purely dispersive or mixed absorptive-dispersive type of saturating nonlinearities, and appear as excellent candidate materials for self-organization studies in planar resonator. Also, when electrically injected, such resonators acquire gain and a focusing dispersive nonlinearity electrically injected amplifying media. Such structures are studied in INLN/Nice, where results are subject to rapid development [15].

Patterns are expected when the branch of steady homogeneous states exhibits modulation instability (MI) on some limited range of the external parameters. These states are important to the extent that their existence is a necessary condition for the observation of cavity solitons. Recent modeling schemes [16,17] showed that in some particular range of the incident intensity, the input-output characteristics displays MI. More particularly, these calculations predicted that the bistable response of a system with a defocusing nonlinearity exhibits MI on the high reflectivity branch states. The observation of pattern formation such as stripes, rhombi, and hexagons, is obtained when structures are excited in an almost purely dispersive regime at a large detuning from the band-gap edge. Such results have been discussed and described in a previous article [18] and also in Ref. [19]. However, this regime does not appear favorable to the existence of CS, essentially because of the defocusing character of the nonlinearity. Therefore, the vicinity of the band-gap edge of III-V semiconductors where saturable absorption is present

*Electronic address: robert.kuszelewicz@lpn.cnrs.fr

exhibits more favorable optical nonlinear properties [20].

This paper reports on the experimental observation of localized structures investigated in the strong absorption region of the Urbach's tail. There, absorption saturation becomes an important nonlinear mechanism that must be considered on a footing comparable to that of nonlinear dispersion, and localized states are observed as transient or final states of a self-initiated evolution of the optical response, emerging from homogeneous nonlinear steady states. These states appear as bright or dark spots in reflection, with a stable or transient character, and in some cases, even outside the parametric conditions for steady-state bistability. Recently, similar observations have been performed in PTB-Braunschweig, but did not introduce the essential role played by thermal phenomena [21]. Here, we show that these states originate from the counteracting interplay of two nonlinearities, acting on radically different time scales. The first one is the expected free carrier nonlinearity, the second one is produced by the thermal shift of the electronic band-gap properties. A focused attention is thus given to the understanding of the respective roles played by the production and transverse diffusion of heat, and the other transverse mechanisms contributing to the formation of cavity solitons. In this respect, this article is organized as follows. In the second paragraph, after recalling the mechanisms whose cooperation is required to produce self-organization in a resonator, we point out the specificity of III-V semiconductor systems and describe the experimental context of our observations. The third part investigates the experimental conditions required for the formation of localized structures and identifies their existence. The presence of an unexpectedly strong thermal contribution is acknowledged yielding a variety of behaviors of a much larger amplitude than expected. The fourth part is dedicated to the interpretation of these results: we confront our observations to the thermal hypothesis, thanks to a model coupling the Fabry-Perot equation for the field and the temperature diffusion equation. Finally, a connection with true cavity solitons is introduced leading to the concept of dressed solitons.

II. THE PRINCIPLES AND THE EXPERIMENTAL SYSTEM

A. Mechanisms of self-organization

In translation-invariant structures such as plane resonators, one usually seeks for solutions governed by the same symmetry. However, even with a PW excitation, the interplay between third-order nonlinearities, such as absorption saturation or positive Kerr-like dispersion, and transverse effects, such as light diffraction of free-carrier diffusion, can produce a spontaneous breaking of symmetry of the optical response through the onset of a Turing—or modulation—instability. This phenomenon destabilizes the homogeneous response of an optical system with respect to transverse spatial modulation at the benefit of a structured transverse distribution. The latter may eventually acquire a periodic character. In the presence of an MI, another category of inhomogeneous response is also expected. It corresponds to stable localized states, bright in transmission, which can be inscribed by a transient and localized excitation at an arbitrary location in the transverse plane. Several of these states may coexist without interacting. They have been called cavity solitons in order to distinguish them from—but also in order to refer to—the solutions of the nonlinear Schröedinger equation (NLSE), i.e., temporal or propagative solitons.

Propagative solitons can be generated when a compensation between light diffraction that tends to spread out a light beam, and a focusing Kerr-like dispersive nonlinearity that confines it is met. This situation, mathematically described by the nonlinear Schröedinger equation, has stable solutions when light propagates with a single transverse dimension, but propagative solitons with two transverse dimensions are not stable solutions of the NLSE. On the other hand, the adjunction of a cavity is equivalent to folding the propagation path of a beam. This brings in the additional mechanism of optical feedback that allows a complete stabilization of a CS. A CS appears in a dissipative structure and solely in the presence of MI on the higher excitation branch of the input-output characteristics. It can be inscribed (by a writing beam) over a homogeneous background (the holding beam) through a procedure that corresponds to a local bistable switching mechanism. As such, CS can be considered as binary state elements for all-optical information processing applications. Moreover, CS can be controlled and manipulated by phase or amplitude gradients that can be printed on the holding beam. In such gradients a CS acquires a velocity proportional to the local gradient and moves towards its maximum [9]. This is a key property for designing new devices relying on concepts such as reconfigurable optical memory arrays as well as cellular architecture processors.

B. Microresonators: Material and structures

In order to study the self-organizing properties of III-V semiconductor microresonators, a sample was designed and grown by MOVPE during a single step growth process. The structure comprises an active nonlinear medium sandwiched between two Bragg mirrors. The back and front mirrors consist, respectively, of 23.5 and 17 pairs of an alternation of $Ga_{0.83}Al_{0.17}As$ and AlAs quarter-wave layers. The active part is a multiquantum well (MQW), comprising 17 wells of 91-Å thick GaAs layers separated by 122-Å-thick $Ga_{0.59}Al_{0.41}As$ barriers. The band-gap edge wavelength is 841 nm and the cavity resonance wavelength λ_c ranges from 5 to 10 nm higher, where absorption is comprised between 1000 cm^{-1} and 3000 cm^{-1}. Indeed, in a 91-Å well, the exciton contribution to the dispersive nonlinearity is weak by comparison with that of free carriers [22]. Due to the growth conditions, the sample exhibits a thickness gradient that we used to fine-tune the incident beam wavelength with respect to the gap edge wavelength. In addition to this long-range gradient, the sample display short-range fluctuations arising from interface roughness with a correlation length on the micrometer scale. The sample finesse we measured lies between 500 and 800 depending on the detuning from the band-gap edge, yielding a resonance peak full width at half maximum that ranges between 0.15 and 0.25 nm. This makes

the sample response sensitive to thickness variations of the order of a single atomic layer [23].

The sample is excited by a beam emitted by an argon-ion-pumped tunable CW titanium-sapphire laser. Due to the absorbing substrate, the temporal and spatial responses of the samples are studied in the reflection mode. The incident laser beam is modulated by an acousto-optic modulator, generating triangular or rectangular shaped optical pulses. Their duration is limited to typically 4 μs in order to avoid or control the thermal nonlinearity. Then, the beam is split into two branches by a half-wave plate and a polarizing beam splitter. The first branch allows us to measure the intensity of the incident beam—taken as a reference—with a 90 ps rise time Si-Avalanche photodiode, while the second focuses the incident beam at normal incidence onto the sample through a $\times 8$ microscope objective. The diameter of the excited zone is set to approximately 25 μm, a value substantially larger than the diffraction length, which is about 4.5 μm. The reflected beam is extracted from the incident beam by the use of a quarter-wave plate and a polarizing beam splitter. It is detected in the time domain by a second photodiode, and in the space domain with a CCD camera. Combining the incident and reflected signals on an oscilloscope, it is then possible to obtain the input and output characteristics and to determine the state of excitation of the sample. Time-resolved images of the near field are captured by a fast intensified charge-coupled device (ICCD) camera with a best temporal resolution of 5 ns.

III. EXPERIMENTAL RESULTS

The use of a fast gated ICCD camera allowed us to sample the spatiotemporal evolution of the resonator response. It was performed with a gating time ranging from 50 ns to 100 ns. Together with the camera the Si-Avalanche photodiode spatially samples the signal at an arbitrary position on the reflected beam profile (generally at the center). We have been able to observe the spontaneous localization of light, sometimes accompanied by the formation of stable persistent structures. The mechanism of localization happened under various excitation conditions with or without bistability. Various morphologies were also observed: intense and small bright spots and single as well as double dark features at the center of the reflected beam profile (Fig. 1).

Localization occurred as a specific phenomenon with both spatial and temporal contributions. Localization could be observed both in a bistable (Fig. 2) and nonbistable regimes (Fig. 4). This means that the effects of localization can be observed evenly when the laser wavelength is lower or higher than that of the cavity resonance. This observation is indeed surprising with respect to the common knowledge on bistability with a negative nonlinear dispersive medium. Moreover, at the center of a bright spot, the local reflectivity may be higher than 100%. This points to a localization or lensing mechanism.

In the nonbistable regime (Fig. 4), the resonance wavelength is lower than that of the beam. Exception made of the initial switching, there is a striking similarity of behavior between this situation and the previously described bistable

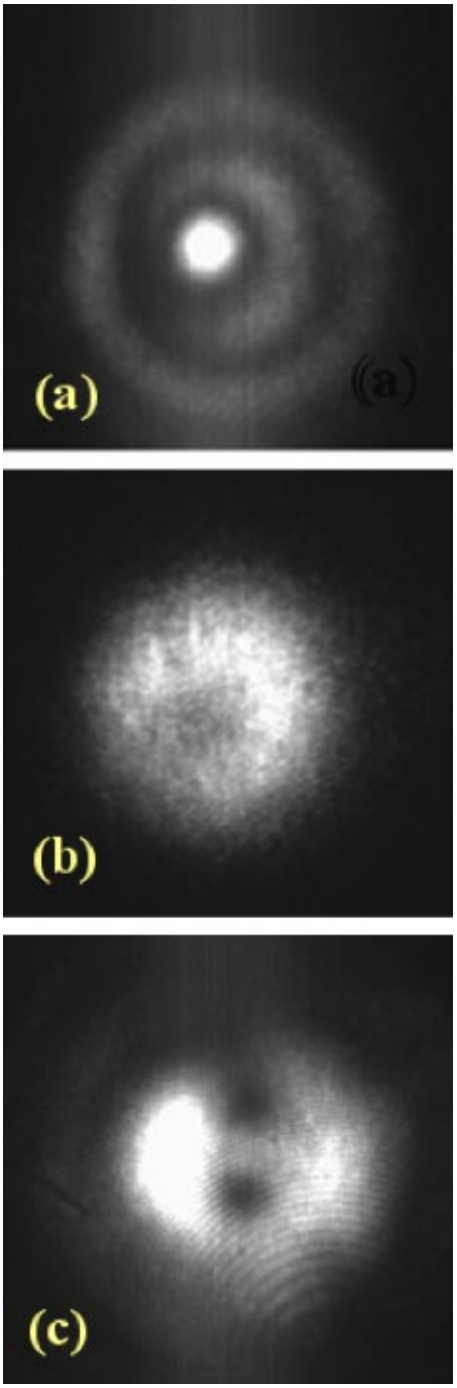

FIG. 1. Various morphologies of localized structures observed after a microsecond time scale: (a) bright and intense spot, (b) single, and (c) double dark spot, at the center of a switched zone. $\lambda_c \simeq 849.6$ nm, $P_{inc} \simeq 40$ mW, diameter $= 25$ μm.

situation. Though no thermal contribution was included, this observation is consistent with the theoretical prediction of coexistence of stable homogeneous states with LS in Ref. [7]. Of a great interest is the observation, during the latter stage of ''destabilization'' of the bright spots, of a relatively dark spot emerging and stabilizing at its center, as in the bistable case (see Sec. IV C).

In the bistable regime (Fig. 2), switching is attested by the

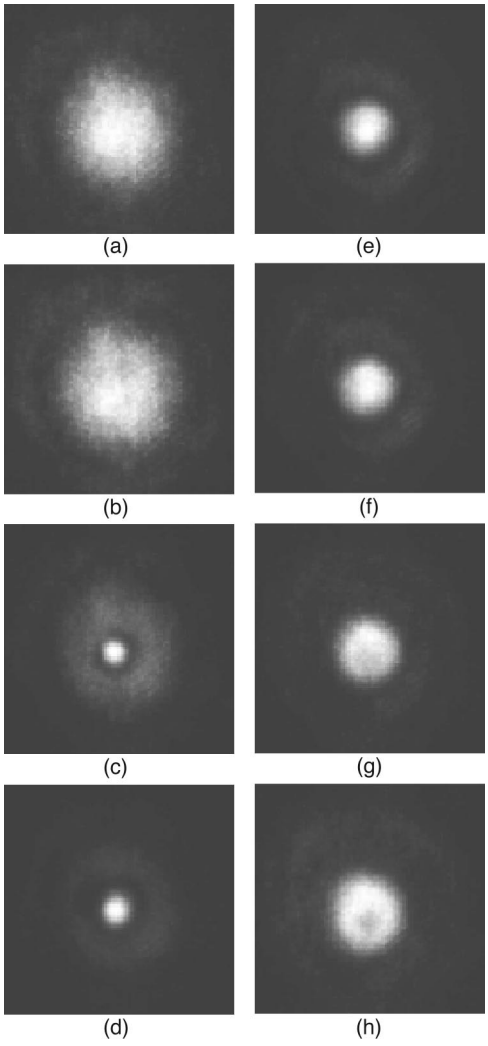

FIG. 2. Spatiotemporal evolution of the reflected beam in a bistable regime. A dark spot stabilizes at the center after the outburst of a bright narrow (~ 10 μm diameter) spot. $\lambda = 849.63$ nm, $\lambda_c = 847.8$ nm, diameter $= 25$ μm, exposure time $= 100$ ns, interval $= 600$ ns.

presence of an external ring which is observable in the dynamical studies and which allows us to identify the branch which each part of the beam refers to. The dynamics of successive states is the following: bistable switching occurs at a very early stage, as the central part of the incident beam crosses the upper threshold: this creates the external most ring; after a slow drift on the microsecond time scale, a very sudden (on the nanosecond scale) concentration of light leads to the formation of a bright and narrow spot in the center, the diameter of which is around 10 μm. This bright spot is not stable and undergoes a spreading phase that leads to the formation of a dark structure at its center. During this process, the existing circular switching fronts do not disappear but rather migrate outwards leading to an accumulation of rings. Fig. 3 reproduces the temporal evolution of the intensity at the center of the reflected beam.

The dynamics of the spectral response was measured experimentally (Fig. 5). It shows the expected redshift of the resonance peak and gives a stronger accuracy to a thermal

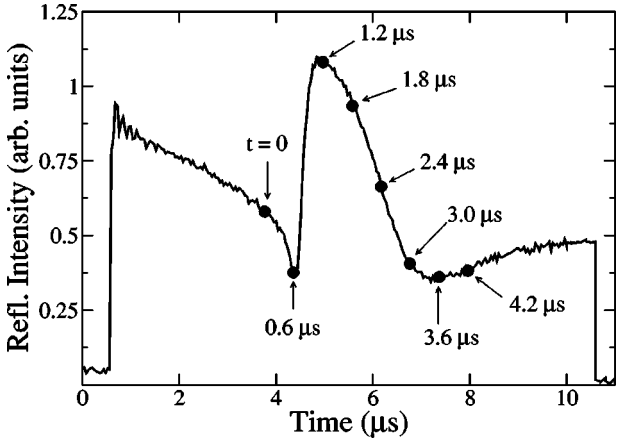

FIG. 3. Time evolution of the reflected signal measured at the center of the spot. The origin of time is taken 4 μs after the onset of the incident illumination.

interpretation. A good qualitative agreement with the redshift of the spectral response instigated by the gap shrinkage is obtained. However, it seems that for a more accurate description, the simplest formulation using a rigid shift must be refined: as the heat accumulated increases, the resonance width sharpens while the contrast decreases. Absorption saturation could be responsible for the apparent increase of the finesse. On the other hand, the decrease of the contrast could be the consequence of an increasing departure from the impedance matching condition [24].

IV. INTERPRETATION OF RESULTS

A. Descriptive model

The results we have obtained lend themselves to a description by a rather simple model which extends the PW description of the nonlinear Fabry-Perot resonator response to the case of a Gaussian illumination. It allows the calculation of the reflected beam amplitude and phase which in turn allows the representation of the spatial phase distribution in the various regions concerned by spatial switching or local heating. This model is phenomenological in the sense that no transverse electronic and optical effect is accounted for and the system is considered as a juxtaposition of uncoupled resonators. The local index is a function of the sole intensity distribution. Heat is considered as introducing a spectral shift leading to an index change proportional to the temperature rise. Our model incorporates the equation of temperature diffusion, that enables us to analyze the electro-thermal nonlinear dynamics. Let us consider a Fabry-Perot resonator with cavity length L, containing a nonlinear material of index n and absorption coefficient α. Front and back mirrors have the respective reflectance R_F and R_B. The cavity reflection coefficient R has the well-known expression [25],

$$R = \frac{R_{min} + F \sin^2 \phi}{1 + F \sin^2 \phi}, \tag{1}$$

where

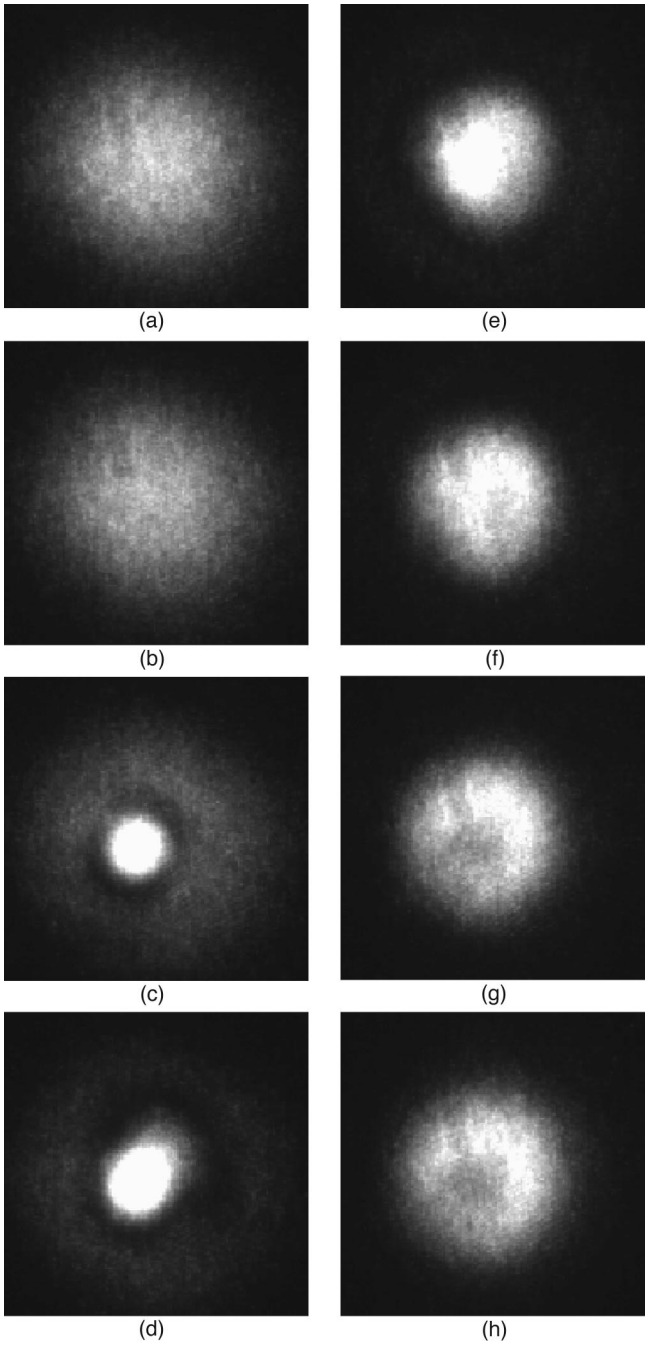

FIG. 4. Spatiotemporal evolution of the reflected beam in a nonbistable regime. A dark spot stabilizes at the center after the sudden burst of a bright narrow spot. $\lambda = 848.1$ nm, $\lambda_c = 847.6$ nm, diameter $= 25\ \mu$m, exposure time $= 100$ ns, interval $= 400$ ns.

$$R_{min} = \frac{(R_F - R_\alpha)^2}{R_F(1 - R_\alpha)^2} \tag{2}$$

is the minimum reflectance reached at $\phi = 0$, and

$$F = \frac{4R_\alpha}{(1 - R_\alpha)^2} \tag{3}$$

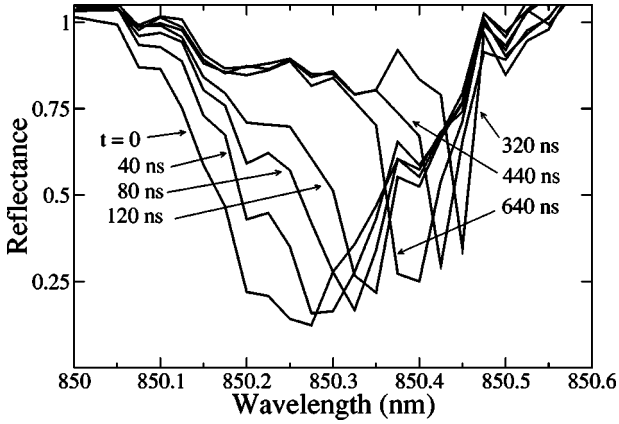

FIG. 5. Spectral response at the center of the beam for a time delay elapsed since the onset of the excitation ranging from 0 to 640 ns.

is the cavity enhancement factor related to the cavity finesse. R_α is defined as

$$R_\alpha = \sqrt{R_F R_B}\exp(-\alpha L). \tag{4}$$

$\phi = \phi_l + \phi_{nl}(I) + \phi_T(T)$ is the single pass total phase shift that contains the linear and intensity-dependent nonlinear contributions, respectively, ϕ_l and $\phi_{nl}(I)$. In the presence of a temperature increase, the total phase contains the additional term $\phi_T(T)$ stemming from the refractive index dependence on temperature. In our experimental situation, $\phi_{nl}(I) < 0$ while $\phi_T(T) > 0$.

The process through which it occurs is illustrated in the bistable case of Fig. 6, where we considered for calculations the thermal index change $\Delta n = 2.10^{-4}\Delta T$ [26].

Under the increase of intensity at short time scales the spectrum deforms and eventually leads to switching. The increase of the intracavity intensity heats the sample. A thermal drift on first approximation brings a rigid shift of the whole NL spectrum. The operating point thus moves back towards resonance. If the temperature increase is large enough, it can

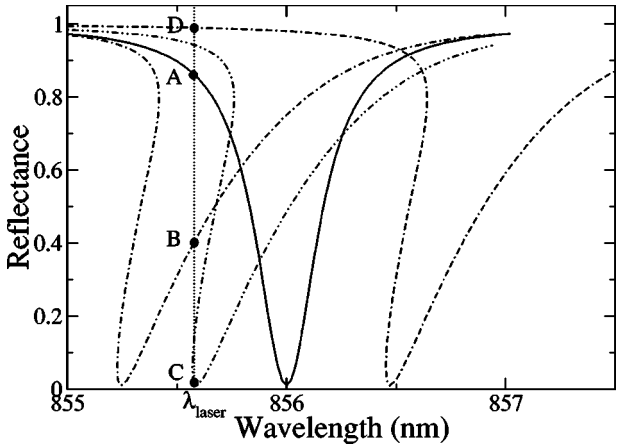

FIG. 6. Evolution of the operating points of a bistable system under the spectral modifications due to a thermal drift. Fast switching from *A* to *B* is followed by a slower evolution to *C* and eventually a fast switching back to *D*.

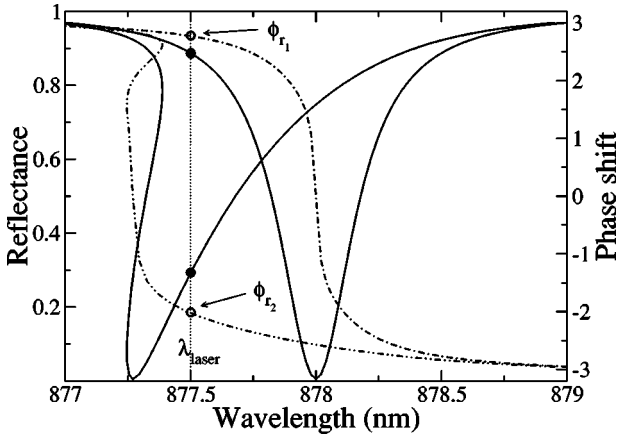

FIG. 7. Spectral dependence of the phase of the reflected field in linear and nonlinear regimes.

switch back to the original high reflectivity state, where a cooling process and a blueshift starts on anew. At small cavity detuning, the hysteresis width is narrow enough to allow the phenomenon to cycle into a regenerative pulsation mechanism (Hopf instability) [27]. At larger detuning, in the bistable case, the larger hysteresis width may prevent cycling from occurring. Then, thermal effects may produce different outcomes that clearly reject the picture of a positive nonlinearity that would simply oppose the negative carrier-generated nonlinearity. This is experimentally observed in the case of a positive cavity detuning. Thermal nonlinearities depicted as a positive nonlinear shift would lead to switching from a high to a low reflectivity state. Instead, one sees a slow, global decrease of intensity, followed by a fast switching towards a high reflectivity state. This frames into the picture we adopted assuming a resonance deformed by a negative nonlinear contribution—because carriers are created in any case—drifting back under a thermal contribution, just as occurs in the second stage of regenerative pulsations.

Along with the spectral dependence of its amplitude, reflectance undergoes also a phase shift as the incident wavelength crosses the resonance peak. Our interpretation in terms of shifting the resonance peak implies that each switching front caused by a thermal drift introduces an additional phase shift of the order of 2π in absolute value (Fig. 7). This information can only be accessed by interferometric techniques. For such a purpose we produced an interference pattern between the reflected beam and a fraction of the incident beam used as a phase reference. In this scheme, an original interference pattern made of linear fringes, can be distorted by the nonlinear index-induced phase shift. The sign of the shift indicates whether the major nonlinear contribution is of electronic or thermal origin and at least allows us to identify the branch on which the system, locally, has its state. This technique is used to identify the various parts of a complex pattern.

B. Thermal mechanisms

As for pattern and CS formation, temperature was not initially considered as a relevant parameter. The use of semiconductor and the experimental evidence reported above have assessed the need for introducing this parameter. Moreover, the thermal contribution must be accounted for in the details of its intimate interaction with the optical response properties of direct gap semiconductors. The conclusions drawn from this analysis will in turn suggest several solutions for avoiding or neutralizing these effects.

We observe that the dynamics result from a combination of fast transients and slower evolutions, the latter allowing the former through an exploration path in the parameter space. Though complex, this situation strongly suggests an interplay between the purely ''carrier-generated'' nonlinear susceptibility and the thermally-induced shift of the index spectrum usually considered as a focusing contribution to dispersive nonlinearity. In semiconductor resonators excited on the Urbach's tail of absorption, heat acts through the change of the lattice parameter and is generally considered as a mechanism that redshifts the band gap. With respect to our spectral range of operation, we may consider the shift of the susceptibility spectrum as rigid. This phenomenon occurs in superposition to the electronic nonlinearity. Therefore, one cannot simply consider thermal effects as a regular dispersive nonlinearity with sign opposite to that of the carrier-generated nonlinearity, but rather as a mechanism causing the drift of the electronic nonlinear properties. In this respect, the positive sign of the contribution of heat to the nonlinear index derives directly from the spectral variation of the dielectric function, at the wavelength of operation, i.e., presently on the band gap (Urbach's) tail. Moreover, the typical time scale of the thermal nonlinearity that stems from heat diffusion is several orders of magnitude slower than that of the fast electronic contribution. The fundamental difference between the two sources of index shift was depicted in the spectral response of a nonlinear Fabry-Perot resonator in Fig. 6. Starting at a low incident intensity from an initially symmetric cavity resonance peak, the increase of the incident intensity produces, through the fast ''electronic'' dispersive nonlinearity, the blueshift and the distortion of the resonance. An incident intensity above threshold yields a nonlinear effect capable of switching the operating point from the high-energy side to the low-energy side of the cavity resonance. Under the progressive temperature increase of the material, occurring on a longer time scale, the distorted peak starts to redshift, causing the operating point to drift along the side of resonance towards its peak, and to eventually switch back to the other side of resonance (Fig. 8).

As moving across a resonance corresponds to shifting the phase of the output signal (Fig. 7), switching can be detected by a phase sensitive experimental technique such as the observation of the pattern produced by the interference between the reflected and incident beams. This is the technique we used to attribute the various parts of annular patterns produced along with localized states a phase. In order to define a reference pattern, we consider the peripheral part of the fringe pattern as corresponding to that of the linear response and use it to evaluate the displacement of the fringes in the central area. In Fig. 7, as one moves along a vertical diameter from the periphery towards the center, one notices a first shift corresponding to the free carrier dispersive effects coinciding

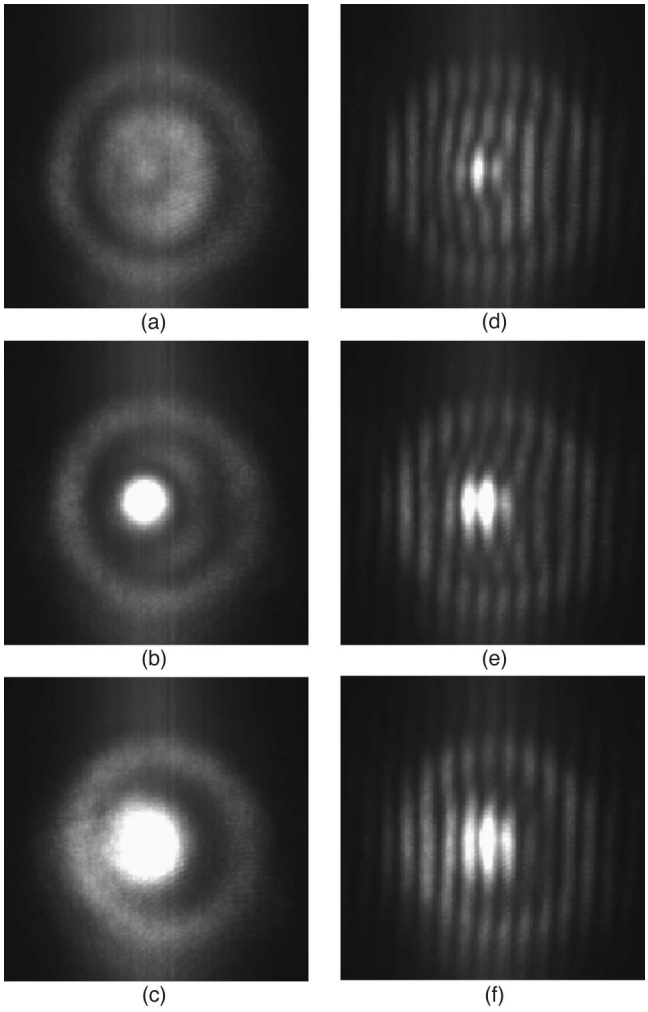

FIG. 8. Phase dynamics of the various parts of a switched beam. The sign of the spatial shift of the fringes gives the spatially resolved phase of the reflected beam. $\lambda = 851.24$ nm, $\lambda_c = \lambda - 0.7$ nm, diameter $= 30\ \mu$m, exposure time $= 50$ ns; images were recorded, respectively, at $t = 0$, 0.8, 1.8 μs.

with the external most switching front. The bright central part bursts in when the intensity reaches its peak at $t = 1.2\ \mu$s (Fig. 3), as a second phase shift occurs, defining a second switching front. As the shift cannot be larger than 2π, because in this spectral range there is no other cavity resonance, it is necessarily opposite to the initial shift, and therefore the observation corresponds to switching back to the high-energy side of the cavity resonance. Finally, as the central bright spot spreads outwards, the second switching front disappears leaving a fringe pattern almost linear in central part. This technique appears very powerful to identify the spatial distribution of states with respect to the high- and low-energy branches. In any situation, this brings an unambiguous confirmation of the mechanisms of carrier-generated versus thermal spatiotemporal nonlinear interplay.

C. Analysis of results

We proceeded in two steps. We used primarily the static model with an arbitrary distribution of temperature, trying to reproduce that of the system, in order to appreciate raw effects. Then, for a more accurate dynamical analysis, in order to account for the transverse interaction mediated by heat, the following equation for heat diffusion was used:

$$\frac{\partial T}{\partial t} = \frac{\alpha I q}{C_{cal}\tau_{nr}} + D_T \nabla_\perp^2 T, \tag{5}$$

where q is the fraction of the carrier density contributing to the heat process. We retained the value $q = 0.2$ that fits most accurately our results. C_{cal} is the heat capacity, D_T is the thermal diffusion coefficient and τ_{nr} is the nonradiative recombination carrier lifetime. The latter mechanism is assumed to give the essential contribution to heat generation via the electron-phonon interaction. The typical values of these parameters for GaAlAs semiconductors are $C_{cal} = 1.8\ \mathrm{J\,K^{-1}\,cm^{-3}}$, $\tau_{nr} = 6$ ns and $D_T = 0.25\ \mathrm{cm^2\,s^{-1}}$. The index change is kept at the value $\Delta n = 2.10^{-4}\Delta T$. In this equation, we assumed that the heat is generated by a density of carriers in equilibrium with the intracavity field intensity I that in the mean field approximation reads [25]

$$I = K \frac{I_{inc}}{1 + F \sin^2 \phi}. \tag{6}$$

The longitudinal contribution of the Laplace operator has been omitted on behalf of the strong thermal resistance generated by the large number of interfaces through which heat must flow. We have therefore assumed that the strongest interaction occurs in the transverse directions. With the help of Eqs. (1), (6), and (5), we proceeded to a comparison with experimental results in two characteristic situations.

1. Bistable regime

In the regime of bistability, for a central bright spot to be observed, a strong thermally induced phase shift must be considered [Fig. 10(a)]. One of the most sizeable effects of a temperature rise is the modification of the local upper and lower bistable thresholds due to a corresponding modification of the local detuning from resonance. Here it was calculated with a maximum temperature rise of 12 K estimated on the basis of the procedure developed in Ref. [28], and accounting for the much higher finesse of the present resonator. The properties of the optical response distribution depend on the current local state and the local values of the thresholds. Comparison of the spatial variation of higher and lower switching thresholds with the intensity profile of the incident beam (Fig. 9) allows determining which part of the incident beam remains below the modified lower threshold and which will switch to the low reflectivity state. Three zones are defined and only the very central part of the initially switched region remains below the lower threshold. This situation forces the switching back of this region to the high reflectivity branch, and makes an additional bright and narrow spot appear in the center of the reflected beam. The beam therefore bears this division into three regions of, respectively, high, low, and again high reflectivity, when moving from the periphery to the center. The time evolution of the reflected

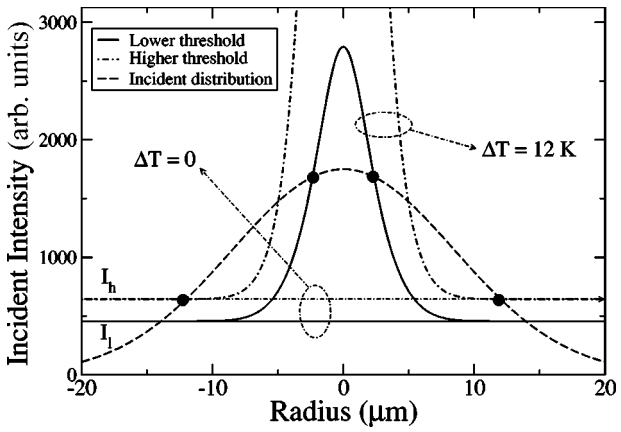

FIG. 9. Dynamics of self-localization: transverse distribution of the low (I_l) and high (I_h) bistability thresholds as thermally altered by a static intensity distribution. The relative values of the thresholds and the incident distribution determine three zones that alternate low and high reflectivities.

field derived from integrating the temperature equation, is sketched in Fig. 10(b), where the successive formation of bright and dark regions, emerging from the switching of the central part of the reflected beam is demonstrated. This approach as it excludes transverse effects such as thermal lensing, cannot account for the overintensity observed experimentally in very bright spots. However, it gives a rather accurate mechanism for the onset of electronic versus thermal nonlinear interplay. To some extent, the mechanism depicted here is a spatial transposition of Hopf instability: with sufficiently large beam, the formation of a larger number of alternately switched zones can be predicted.

The dynamical evolution [Fig. 10(b)] of the intensity distribution reconstructs quite closely the time evolution observed experimentally. In a first stage, the central switched zone reduces until the very center reaches a minimum as resonance is met. At this stage, the reflected intensity increases abruptly, starting from the center. This situation corresponds to the bright localized state observed experimentally. The evolution that follows confirms the expansion of this bright part until a new dark state appears again at the center. The main difference with the experiment lies in the fact that the oscillatory character of the successive states reached at the center does not cease. This can be most probably attributed on the theoretical side to the omission of carrier diffusion and light diffraction that otherwise damps the process and finally stops it.

2. Nonbistable regime

Another confirmation of the thermal analysis is also brought in the following case by the observation of localization in the situation of a nonbistable response, i.e., when the cavity detuning is positive. The corresponding experimental situation was exposed in Fig. 4. Despite of the nonbistable response, a stronger incident intensity can induce a higher temperature increase. The succession of states at the center of the beam is sketched on Fig. 11(a). From state *A* on the high-energy side of resonance, the system moves to *B* as the

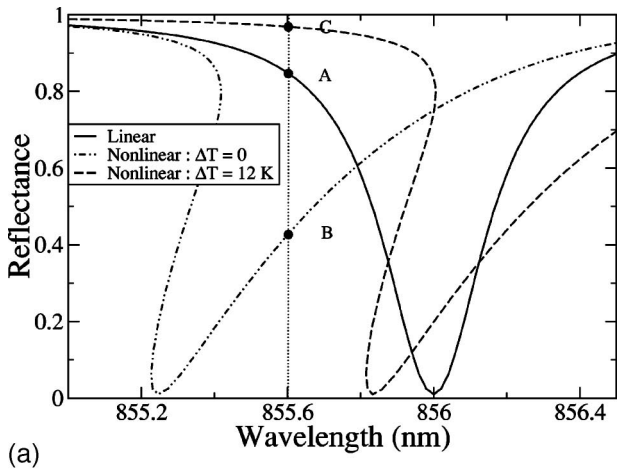

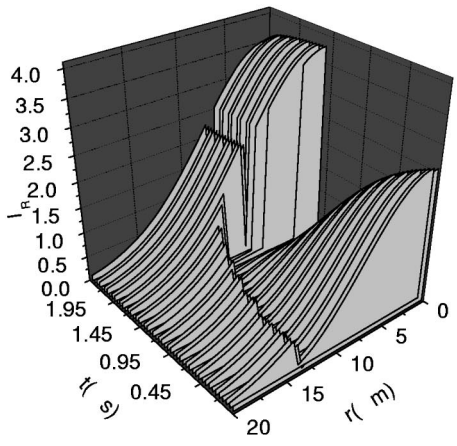

FIG. 10. Dynamics of self-localization: (a) static model, shift of the reflectivity spectrum at the beam center, under a temperature increase of 12 K. Calculations are performed with experimental parameter values. (b) Spatiotemporal evolution of the transverse distribution of the reflected intensity.

temperature increase redshifts the resonance. Finally, as in the bistable case, the system can switch to a high reflectivity state. The dynamics of the temperature distribution, calculated by solving the diffusion equation, is sketched on Fig. 11(b).

D. Dressed cavity soliton

The previous results have shown the emergence of solitary localized states. They raise, however, the question of the connection of these localization effects with those expected from the theory of solitons. All the examples shown above apparently concern the central part of the beam and can be, to a very large extent, explained by PW bistability arguments transposed to an inhomogeneous profile. However, this type of description is not sufficient to account for the existence of high concentration of light, where the lack of transverse mechanisms is obvious. One could also object that the spot center being also the maximum of amplitude profile where the gradient vanishes, there are great chances that any localized structure created in the neighborhood would converge

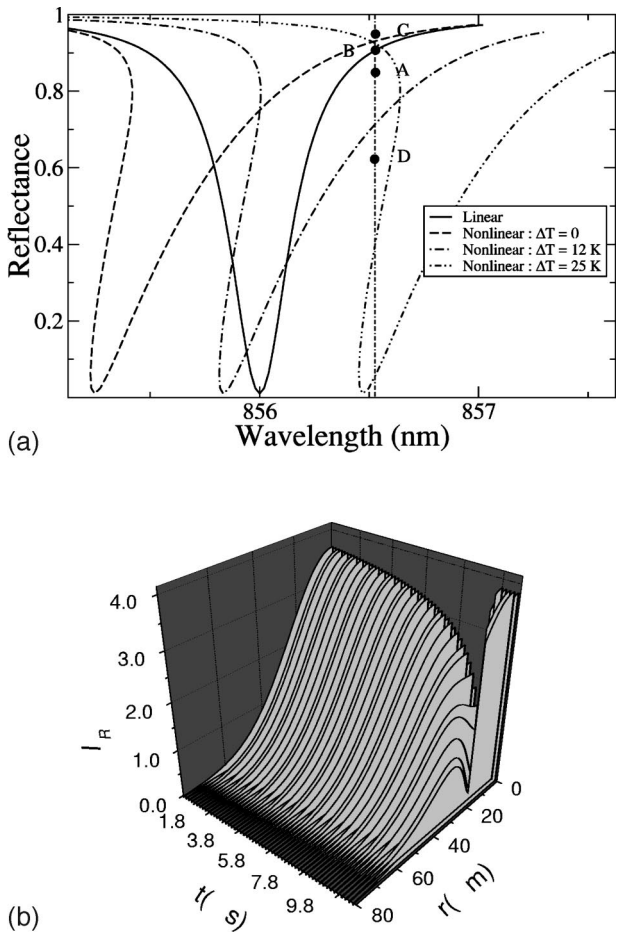

FIG. 11. (a) Distribution of the reflected beam at the start (dashed) and at the end (solid) of the thermal drift in the nonbistable regime. (b) Dynamical evolution of the intensity distribution, in the nonbistable regime.

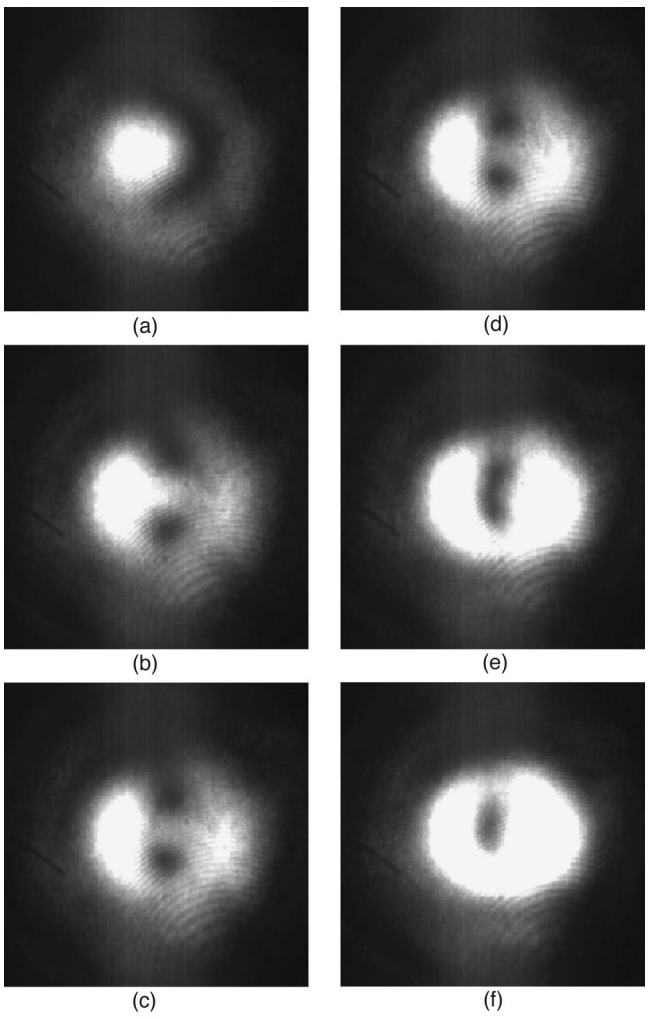

FIG. 12. ICCD image sequence of the reflected beam under the following excitation conditions, diameter= 20 μm. Images were recorded, respectively, at $t=0$, 100, 200, 300, 400, and 700 ns after the central bistable switching.

there in a very short time scale. However, in view of the interpretation developed in this article, it seems difficult to attribute the full quality of cavity soliton to the states we have observed. Similarly, the observations reported in the meantime in Ref. [29] on a quite similar system cannot be considered as cavity solitons as they are claimed to be. A first argument is that according to the most reliable theory [20], such a system cannot host simultaneously bright and dark cavity solitons. A second point is that with such excitation conditions it is not possible to avoid accounting for a thermal contribution (Fig. 5).

The last set of results we present depicts the simultaneous emergence of two dark localized states. The sequence of images on Fig. 12 shows the spontaneous appearance of two black spots out of center. Their size is typically 5 μm. They move to the center, without interacting. Finally, when they get close enough to each other, they start interacting and merge into a single structure. In this particular situation, most of the properties required for qualifying a cavity soliton are met, except for the spontaneous character of their onset. For instance they are dark in reflection, their size seems rather constant unless they interact, they move towards the center as if they were driven by the intensity gradient of the incident beam and finally they merge into a single structure of the same size. The main difference though lies in the fact that this double structure appears spontaneously. This brings an important objection. Though, if one considers temperature as a scanning parameter, exploring locally the parameter space, one can introduce the concept of a soliton dressed by thermal mechanisms. This viewpoint introduced among partners of the PIANOS project is rather powerful since it allows using the theoretical properties of bare solitons, perturbed by an external mechanism. This concept can be used for theoretical as well as experimental approaches and even enlarged so as to include other external effects such as thickness resonance induced by thickness fluctuations.

V. CONCLUSION

In this article, we have presented a set of results obtained on semiconductor microresonators and contributing to the demonstration of self-organizing properties of light-matter interaction. III-V semiconductors have shown to constitute a

very promising material for investigating this new category of states. Localized states were observed with properties partially meeting those expected from cavity solitons. We subsequently demonstrated that they are strongly ruled by thermal mechanisms, where heat was shown to act mostly as a dressing mechanism that screens the bare soliton properties. Actually, efforts in the theory conducted in INFM/Milan-Bari and in University of Strathclyde or Glasgow are directed at the incorporation of the temperature as a canonic parameter. This should contribute to a better prediction of parameter ranges for soliton stability. On the other hand, our experimental effort tends to the mastering of heat mechanisms through all aspects: production, dissipation, and dressing effects. To this extent, it is quite clear that material and cavity engineering are of the highest concern.

ACKNOWLEDGMENT

This work has been partially funded by the European Commission through the LTR ESPRIT Project No. 28235 PIANOS.

[1] A. Szoke, D. Daneu, J. Godhar, and N.A. Kurnit, Appl. Phys. Lett. **15**, 369 (1969).
[2] J.H. Marburger and F.S. Felber, Phys. Rev. A **17**, 335 (1978).
[3] R. Bonifacio and L.A. Lugiato, Phys. Rev. A **18**, 1129 (1978).
[4] R. Kuszelewicz, J-L. Oudar, J-C. Michel, and R. Azoulay, Appl. Phys. Lett. **53**, 2138 (1988).
[5] H.M. Gibbs, *Optical Bistability: Controlling Light with Light* (Academic, New York, 1985).
[6] L.A. Lugiato, M. Brambilla, and A. Gatti, Adv. At., Mol., Opt. Phys. **40**, 229 (1998).
[7] M. Tlidi, P. Mandel, and R. Lefever, Phys. Rev. Lett. **73**, 640 (1994).
[8] M. Brambilla, L.A. Lugiato, F. Prati, L. Spinelli, and W.J. Firth, Phys. Rev. Lett. **79**, 2042 (1997).
[9] W.J. Firth and A. Scroggie, Phys. Rev. Lett. **76**, 1623 (1996).
[10] M. Tlidi, P. Mandel, and M. Haelterman, Phys. Rev. E **56**, 6524 (1997).
[11] C.O. Weiss, Report No. 21112, 1996 (unpublished).
[12] V.B. Taranenko, K. Staliunas, and C.O. Weiss, Phys. Rev. A **56**, 1582 (1997).
[13] B. Shäpers, M. Feldman, T. Ackemann, and W. Lange, Phys. Rev. Lett. **85**, 748 (2000).
[14] W.J. Firth and G.K. Harkness, Asian J. Phys. **7**, 665 (1998).
[15] S. Barland, J.R. Tredicce, M. Brambilla, L.A. Lugiato, S. Balle, M. Giudicci, T. Maggipinto, L. Spinelli, G. Tissoni, T. Knoedl, M. Miller, and R. Jaeger, Nature (London) **419**, 699 (2002).
[16] L. Spinelli, G. Tissoni, M. Brambilla, F. Prati, and L.A. Lugiato, Phys. Rev. A **58**, 2542 (1998).
[17] D. Michaelis, U. Peschel, and F. Lederer, Phys. Rev. A **56**, R3366 (1997).
[18] R. Kuszelewicz, I. Ganne, I. Sagnes, G. Slekys, and M. Brambilla, Phys. Rev. Lett. **84**, 6006 (2000).
[19] V. Taranenko, I. Ganne, R. Kuszelewicz, and C.O. Weiss, Phys. Rev. A **61**, 063818 (2000).
[20] G. Tissoni, L. Spinelli, M. Brambilla, T. Maggipinto, I. Perrini, and L.A. Lugiato, J. Opt. Soc. Am. B **16**, 2095 (1999).
[21] V. Taranenko, I. Ganne, R. Kuszelewicz, and C.O. Weiss, Appl. Phys. B: Lasers Opt. **B72**, 377 (2001).
[22] P.K. Milsom and A. Miller, Opt. Quantum Electron. **21**, 81 (1989).
[23] J-L. Oudar, R. Kuszelewicz, B. Sfez, J-C. Michel, and R. Planel, Opt. Quantum Electron. **24**, S193 (1992).
[24] E. Garmire, IEEE J. Quantum Electron. **25**, 289 (1989).
[25] B. Wherrett, IEEE J. Quantum Electron. **20**, 646 (1984).
[26] C. Tanguy, J. Appl. Phys. **80**, 4626 (1996).
[27] K.I. Ikeda, Opt. Commun. **30**, 257 (1979).
[28] R. Kuszelewicz, J-L. Oudar, R. Azoulay, J-C. Michel, J. Brandon, and O. Emile, Phys. Status Solidi B **150**, 465 (1988).
[29] V. Taranenko, C.O. Weiss, and W. Stolz, J. Opt. Soc. Am. B **19**, 684 (2002).